



Providing Choice & Value

Generic CT and MRI Contrast Agents



CONTACT REP

AJNR

This information is current as of July 18, 2025.

Volumetric Measurement of Relative CBV Using T1-Perfusion-Weighted MRI with High Temporal Resolution Compared with Traditional T2*-Perfusion-Weighted MRI in Postoperative Patients with High-Grade Gliomas

M. Seo, K.-J. Ahn, Y. Choi, N.-Y. Shin, J. Jang and B.-S. Kim

AJNR Am J Neuroradiol published online 26 May 2022
<http://www.ajnr.org/content/early/2022/05/26/ajnr.A7527>

Volumetric Measurement of Relative CBV Using T1-Perfusion-Weighted MRI with High Temporal Resolution Compared with Traditional T2*-Perfusion-Weighted MRI in Postoperative Patients with High-Grade Gliomas

 M. Seo,  K.-J. Ahn,  Y. Choi,  N.-Y. Shin,  J. Jang, and  B.-S. Kim



ABSTRACT

BACKGROUND AND PURPOSE: T1-PWI with high temporal resolution may provide a reliable relative CBV value as a valid alternative to T2*-PWI under increased susceptibility. The purpose of this study was to assess the technical and clinical performance of T1-relative CBV in patients with postoperative high-grade gliomas.

MATERIALS AND METHODS: Forty-five MRIs of 34 patients with proved high-grade gliomas were included. In all MRIs, T1- and T2*-PWIs were both acquired and processed semiautomatically to generate relative CBV maps using a released commercial software. Lesion masks were overlaid on the relative CBV maps, followed by a histogram of the whole VOI. The intraclass correlation coefficient and Bland-Altman plots were used for quantitative and qualitative comparisons. Signal loss from both methods was compared using the Wilcoxon signed-rank test of zero voxel percentage. The MRIs were divided into a progression group ($n = 20$) and a nonprogression group ($n = 14$) for receiver operating characteristic curve analysis.

RESULTS: Fair intertechnique consistency was observed between the 90th percentiles of the T1- and T2*-relative CBV values (intraclass correlation coefficient = 0.558, $P < .001$). T2*-PWI revealed a significantly higher percentage of near-zero voxels than T1-PWI (17.7% versus 3.1%, $P < .001$). There was no statistically significant difference between the area under the curve of T1- and T2*-relative CBV (0.811 versus 0.793, $P = .835$). T1-relative CBV showed 100% sensitivity and 57.1% specificity for the detection of progressive lesions.

CONCLUSIONS: T1-relative CBV demonstrated exquisite diagnostic performance for detecting progressive lesions in postoperative patients with high-grade gliomas, suggesting the potential role of T1-PWI as a valid alternative to the traditional T2*-PWI.

ABBREVIATIONS: AUC = area under the curve; CE = contrast-enhanced; ICC = intraclass correlation coefficient; rCBV = relative CBV; ROC = receiver operating characteristic; SSE = substantial susceptibility effects; T1-rCBV = T1-PWI-derived relative CBV; T2*-rCBV = T2*-PWI-derived relative CBV

Perfusion MR imaging is a well-established method used to evaluate the degree of angiogenesis in brain tumors, especially gliomas.^{1,2} Among the various parameters measured in perfusion MR imaging, relative CBV (rCBV) plays a key role in glioma grading,^{3,4} discriminating pseudoprogression and progression of posttreatment glioblastoma,⁵⁻⁸ and predicting future progression.⁹

T2*-PWI, also known as dynamic susceptibility contrast, is the most commonly used technique for the calculation of rCBV.¹⁰ On the basis of T2*-weighted EPI, T2*-PWI provides exponential


signal change and high temporal resolution (<3 seconds per phase) without greatly sacrificing spatial resolution. With frequent sampling of the signal intensity, T2*-PWI can be used to draw precise concentration curves for both tissue perfusion and arterial input function, assuring proper deconvolution of parameters. However, because of its high sensitivity to magnetic susceptibility, it is limited by image degradation near the sources of field heterogeneity, such as metallic surgical materials, air-containing anatomic structures, blood products, or calcifications. Some studies reported suboptimal evaluation in postoperative imaging with T2*-PWI due to the increased prevalence of the aforementioned conditions.¹¹⁻¹³

T1-PWI, also known as dynamic contrast enhancement, is another technique based on linear signal change related to T1 shortening of the tissue and is characterized by increased resilience to the susceptibility induced by postsurgical changes. Several attempts were made to calculate CBV by using this method at the advent of perfusion MR imaging.^{14,15} Owing to the relatively low temporal

Received October 13, 2021; accepted after revision April 8, 2022.

From the Department of Radiology, Seoul St. Mary's Hospital, College of Medicine, Catholic University of Korea, Seoul, Republic of Korea.

Please address correspondence to Kook-Jin Ahn, MD, PhD, Department of Radiology, Seoul St. Mary's Hospital, College of Medicine, Catholic University of Korea, 222 Banpo-daero, Seocho-gu, Seoul, 06591, Republic of Korea; e-mail: ahn-kj@catholic.ac.kr

 Indicates article with online supplemental data.

<http://dx.doi.org/10.3174/ajnr.A7527>

resolution of many T1-PWI acquisition techniques, however, arterial input functions may be insufficient, leading to unreliable perfusion metrics, especially when scanning the whole brain with source images of acceptable quality. Narrow coverage and thick-section imaging may increase the temporal resolution, though some tumor information may be missed.

With the recent widespread application of MR imaging acceleration techniques, several studies have assessed the clinical utility of T1-PWI-derived rCBV.^{13,16–22} However, few studies have focused on its usefulness for postoperative imaging, the most typical susceptibility-prone situation.^{13,17} Only 2 studies provided histogram analysis,^{19,22} while others used maximal rCBV values within the radiologist-drawn ROI. Most of the studies used their own in-house software due to the lack of an optimized commercial program, which provides established theoretic accuracy but is difficult for other investigators to reproduce. In the current study, we conducted a postoperative volumetric analysis of T1-PWI-derived rCBV (T1-rCBV) using readily available software, achieving a temporal resolution of 2.2 seconds with whole-brain coverage, and ensuring image quality.

Therefore, the purpose of this study was to assess the technical and clinical performance of T1-rCBV, scanned and measured with a high-temporal-resolution protocol in postoperative patients with high-grade gliomas using commercially released software as a valid alternative to the traditional T2*-PWI.

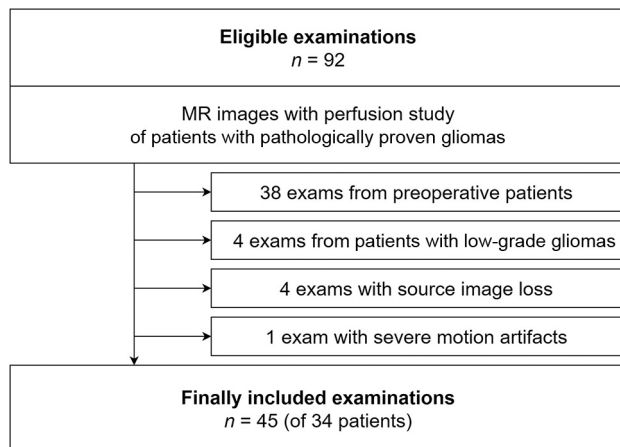


FIG 1. A flow chart outlining the selection of patients and examinations is shown.

MATERIALS AND METHODS

Study Population

This retrospective study was approved by our institutional review board. Informed consent of enrolled patients was waived due to its retrospective nature.

In our PACS, we identified MR imaging studies, including perfusion scans, performed in patients with pathologically proved high-grade gliomas from April 2018 to January 2021. Among 92 MR imaging examinations, 45 examinations of 34 patients were finally included in the study. Figure 1 shows the flow chart for patient selection.

Image Acquisition

All MR images were acquired on a 3T scanner (Ingenia; Philips Healthcare). Routine precontrast sequences included sagittal and axial T1WI, coronal and axial T2WI, axial T2 FLAIR images, axial T2*WI, and axial DWI.

T2*-PWI requires contrast agent preload to avoid the T1 shunt-through effect.^{13,23} Therefore, T1-PWI scans with a time resolution of 2.2 seconds were obtained previously, assisted by sensitivity encoding and accelerated by factors $R = 2.2$ and 1.2 for phase and partition encoding directions (y and z directions), respectively. For both perfusion imaging techniques, 0.1 mmol/kg of gadobutrol (Gadovist; Bayer Schering Pharma) was administered intravenously with an injection rate of 3 mL/s , injecting 4 mL first during the preceding T1-PWI scan, followed by 6 mL for the T2*-PWI scan. Following the perfusion study, 3D contrast-enhanced (CE)-T1WI was acquired with a 3-plane MPR.

The parameters used for key sequences are summarized in Table 1.

Image Postprocessing

All image-processing steps were performed using the commercial software nordicICE (Version 4.1.3; NordicNeuroLab). First, all images were coregistered on the reference image, CE-T1WI. Lesion masks were produced on CE-T1WI using a semiautomatic segmentation tool with the seed-growing method. Visual assessment was used to avoid large vessels and internal content of the surgical cavity, such as fluid, hemorrhage, or necrosis.

For T1-PWI analysis, we used the perfusion analysis module of nordicICE, which was originally more commonly used in T2*-PWI analysis. Signal conversion into a concentration curve was based on $1/T_1$ acquired by spoiled gradient-echo images, rather than R_2^* change versus time. A fixed baseline T1 time (1400 ms) was used during the conversion, referring to recent studies.^{24,25} We

Table 1: Parameters of key MR imaging sequences

	T1-PWI	T2*-PWI	T2WI	T2 FLAIR	3D CE-T1WI
Sequence	3D T1-FFE	3D T2-FFE	TSE	TSE	3D TSE
TR/TE (ms)	4.2/2.3	1800/30	3000/80	9000/100	550/30
Flip angle	8°	40°	90°	90°	90°
FOV (mm ²)	220 × 220	210 × 210	230 × 230	230 × 230	240 × 240
Matrix	137 × 137	128 × 128	404 × 382	308 × 290	240 × 240
Section thickness (mm)	5	5	5	5	1
Slices	30	25	26	26	200
Time resolution (sec)	2.2	1.8			
Phases	150	50			
Note					Black-blood, Dixon fat suppression

Note:—FFE indicates fast-field echo.

also performed motion correction, leakage correction, and model-independent deconvolution by standard singular value decomposition. Pixels for arterial input functions were semiautomatically searched in the circle of Willis, and the peak shapes of all arterial input functions were visually assessed. The high temporal resolution of the T1-PWI scan facilitated the easy selection of appropriate arterial input functions. The WM mask was automatically generated by the software to obtain normalized rCBV values. An identical procedure was performed for the analysis of T2*-PWI source images, except for the signal conversion step.

Lesion masks, representing the VOIs, were overlaid on T1- and T2*-PWI-derived rCBV (T2*-rCBV) maps for histogram analysis of the whole enhancing lesion. Basic statistics of T1- and T2*-rCBV values were recorded for each MR imaging examination, including the mean, median, SD, and 90th percentile.

Statistical Analysis

For each lesion, susceptibility effects and visualization grades were qualitatively evaluated on the basis of a consensus of 2 neuroradiologists (one with >20 years of experience and another with 5 years of experience). A linear T2*WI dark lesion along the surgical margin with <5-mm thickness was regarded as marginal hemorrhage. Hemorrhage measuring >5 mm with apparently defective visualization of the VOI was regarded as considerable hemorrhage. The visualization grade was assessed for all lesions on T1- and T2*-PWI. The grade was defined by visually estimating the fraction of signal loss within the VOI: grade 3 = <20% signal loss, grade 2 = 20%–50% signal loss, grade 1 = 50%–80% signal loss, and grade 0 = >80% signal loss. The results of visualization grading of the 2 methods were compared using the Pearson χ^2 test.

For comparison of T1- and T2*-PWI, the intraclass correlation coefficient (ICC), and the Pearson correlation coefficient *R* were calculated for the 90th percentile and the mean values of the rCBV histogram. On the basis of the 95% confidence interval of the ICC estimate, values were interpreted as follows: ICC < 0.50 = poor, 0.5–0.74 = moderate, 0.75–0.89 = good, >0.90 = excellent.²⁶ Bland-Altman plots were constructed for qualitative assessment of the correlation between T1- and T2*-rCBVs.

Cumulative and noncumulative histograms of rCBV in all VOIs were plotted for visual comparison of rCBV distribution. The number of voxels with an absolute zero value was counted in a voxelwise manner from T1- and T2*-PWI, and the percentage of voxels containing zero-valued rCBV within the whole VOI was calculated in each tumor. The Wilcoxon signed-rank test was performed to quantitatively compare the zero voxel percentages of T1- and T2*-PWI.

Receiver operating characteristic (ROC) curve analysis was used to evaluate the clinical performance, discriminating progression and nonprogression in postoperative examinations. The examination was assigned to a progression group if it included a pathologically confirmed tumor in the reoperation within 3 months or if it revealed a clearly measurable lesion according to Response Assessment in Neuro-Oncology criteria with additional radiologic or clinical evidence of progression within 3 months (clinical progression meant death or obvious deterioration). If the lesion of interest was surgically confirmed to contain <5% viable tumor cells within 3 months or if the lesion was radiologically not measurable

and frank local progression was not observed for the next 6 months, the examination was assigned to a nonprogression group. The areas under the curve (AUCs) calculated from ROC curves of T1- and T2*-rCBV were compared with each other via the DeLong test.

Additional subgroup ROC curve analysis was performed. One subgroup included examinations with substantial susceptibility effects (SSE, defined as grades 0–1; ie, <50% visualization on T2*-PWI), and another subgroup included examinations without SSE (grades 2–3; ie, >50% visualization on T2*-PWI). ROC curves were drawn, and AUC values were calculated in each subgroup.

All statistical analyses were performed using an open-source statistical language (R Studio, Version 1.4.1106; <http://rstudio.org/download/desktop>). A *P* value ≤ .05 was interpreted as statistically significant.

RESULTS

The overall characteristics of the 45 examinations of 34 patients are shown in the Online Supplemental Data. All patients were at least once surgically diagnosed with high-grade glioma before or during the study period. Among them, 24 patients were eventually diagnosed with grade 4 lesions, and another 10 patients eventually exhibited grade 3 lesions. During the study period, 8 patients had undergone multiple perfusion MRIs.

Among 45 examinations, 15 examinations (33.3%) were conducted within 6 months of the operation. In 9 examinations, the VOI was located at the skull base area, with mild or considerable susceptibility effects by location. More than 90% of the cases showed marginal or considerable hemorrhage because all examinations were postoperative MRIs. Only 13 lesions were fully visible (28.9%, grade 3) on T2*-PWI, while another 32 lesions were suboptimal (71.1%, grades 0–II). Nine T2*-PWIs were difficult to interpret due to SSE, meaning that half or more of the VOI was shaded by signal loss (20%, grades 0–I). One sample case of grade 1 visualization is presented in Fig 2, and 2 more illustrative sample cases are presented in the Online Supplemental Data. On the other hand, only 4 lesions were suboptimally visualized (8.9%, grades 0–II), while other lesions were fully evaluated on T1-PWI (91.1%, grade 3). The Pearson χ^2 test revealed significant differences in the visualization grade between the 2 methods (*P* < .001).

The scatterplot of T2*-rCBV versus T1-rCBV is presented in Fig 3. For both the 90th percentile and the mean of the whole lesion, rCBV measurement showed fair intertechnique consistency (ICC = 0.558 and 0.566, respectively, both *P* < .001). Additionally, Pearson correlation analysis revealed a significant positive correlation of the 90th percentile and mean values (*R* = 0.614 and 0.663, respectively, both *P* < .001) between the 2 methods. In 39 examinations, the 90th percentiles of rCBV were within the limits of agreement on the Bland-Altman plot (Fig 4), displaying 4 upper and 2 lower outliers.

T1- and T2*-rCBV values of all lesions of interest were drawn as a cumulative histogram (Fig 5), with the T2*-rCBV curves more frequently showing a higher initial cumulative fraction of near-zero voxels than the T1-rCBV curves. Noncumulative histograms of both methods can be found in the Online Supplemental Data. The mean percentages of zero-valued voxels within VOIs were 3.1% and 17.7% in T1- and T2*-PWI, respectively, demonstrating a significant difference (*P* < .001).

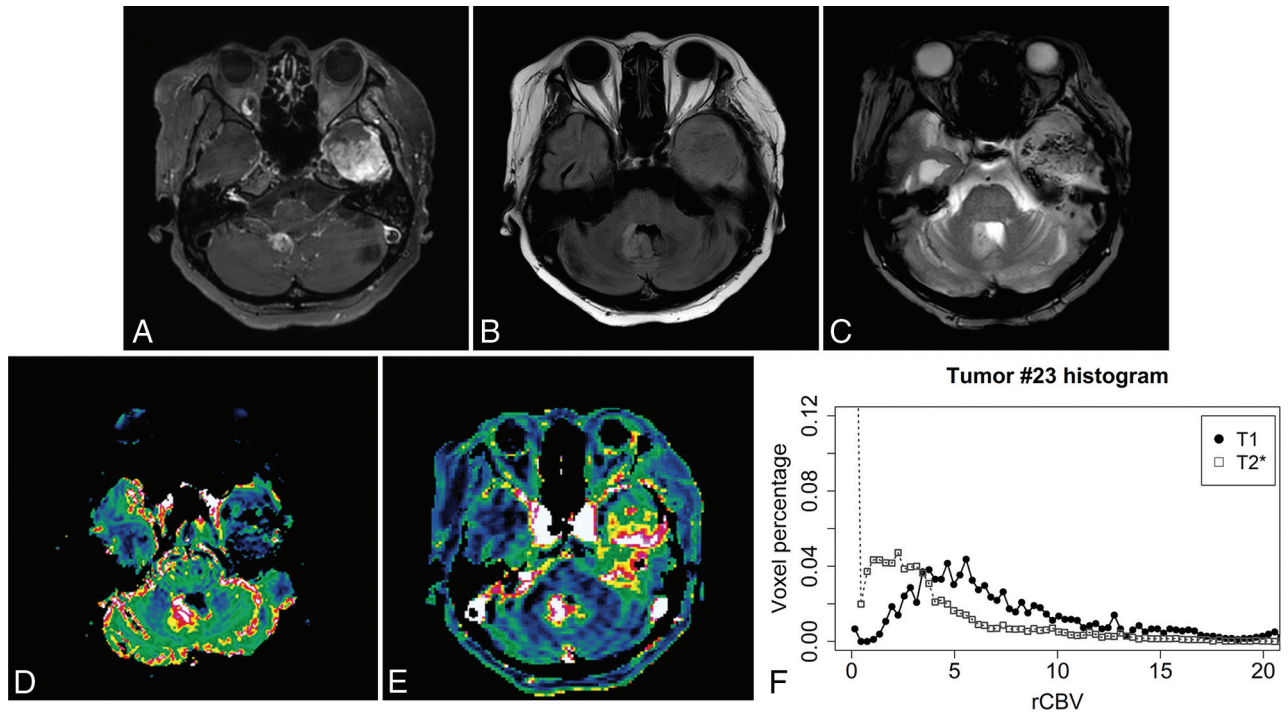


FIG 2. A 53-year-old woman with primary glioblastoma located in the left thalamus. On the follow-up image 10 months after the operation (7 months after the last radiation therapy), new enhancing lesions are noticed in the left temporal lobe base and fourth ventricle (A and B). Owing to its location and considerable amount of internal hemorrhage (C), signal loss shades the portions of the left temporal lobe lesion, resulting in grade 1 visualization on T2*-PWI (D, rCBV 90th percentile, 8.18). Grade 3 visualization is achieved on T1-PWI (E, rCBV 90th percentile, 23.92). Susceptibility-induced signal loss of the T2*-PWI is also well-noticed on the histogram, with the leftmost peak of near-zero voxels (F). The patient died in 1 month and was assigned to the progression group on ROC curve analysis.

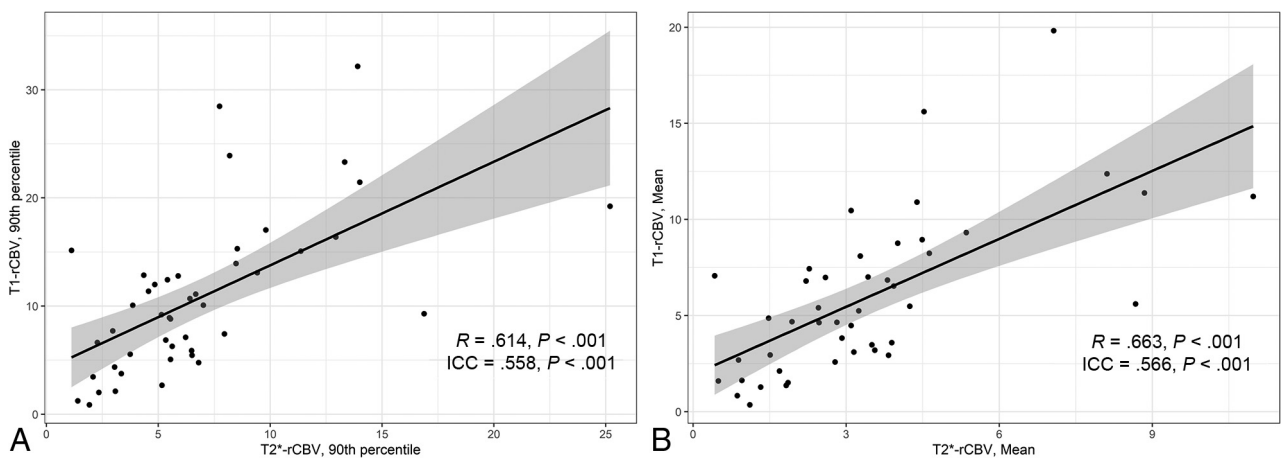


FIG 3. Scatterplots of rCBV values derived from T1- and T2*-PWI. A, Ninetieth percentile of the whole lesion rCBV values, with fair consistency (ICC = 0.558) and a positive correlation ($R = 0.614$). B, Mean of the whole-lesion rCBV values, with fair consistency (ICC = 0.566) and a positive correlation ($R = 0.663$).

The 90th percentiles of T1- and T2*-rCBV values were both significantly higher in the progression group than in the nonprogression group (Table 2). Boxplots comparing T1- and T2*-rCBV between the progression and nonprogression groups are provided in the Online Supplemental Data. The AUCs of the 90th percentiles of T1- and T2*-rCBV were 0.811 and 0.793, respectively, on the ROC curve presented in Fig 6, with no significant difference ($P = .835$). At the cutoff value of 4.930, T1-rCBV was used to detect all eventually progressed tumors, with

100% sensitivity and 57.1% specificity. The optimal cutoff value of T2*-rCBV was 4.453, with 90.0% sensitivity and 64.3% specificity.

According to the subgroup ROC analysis, as shown in the Online Supplemental Data, the AUC of T2*-rCBV was lower than that of T1-rCBV (0.500 versus 0.750, $P = .117$) in the subgroup with SSE. In the subgroup without SSE, on the other hand, the AUC of T2*-rCBV was slightly higher than that of T1-rCBV (0.875 versus 0.824, $P = .597$).

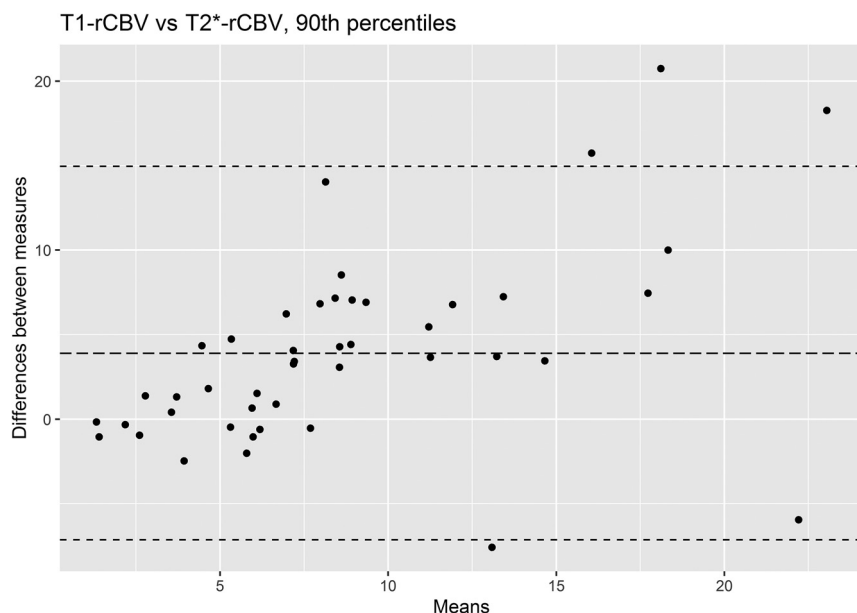


FIG 4. A Bland-Altman plot representing the 90th percentile of rCBV values derived from T1- and T2*-PWI. The upper and lower dashed lines represent the 1.96 and -1.96 limits of agreement, respectively (95% confidence interval not indicated).

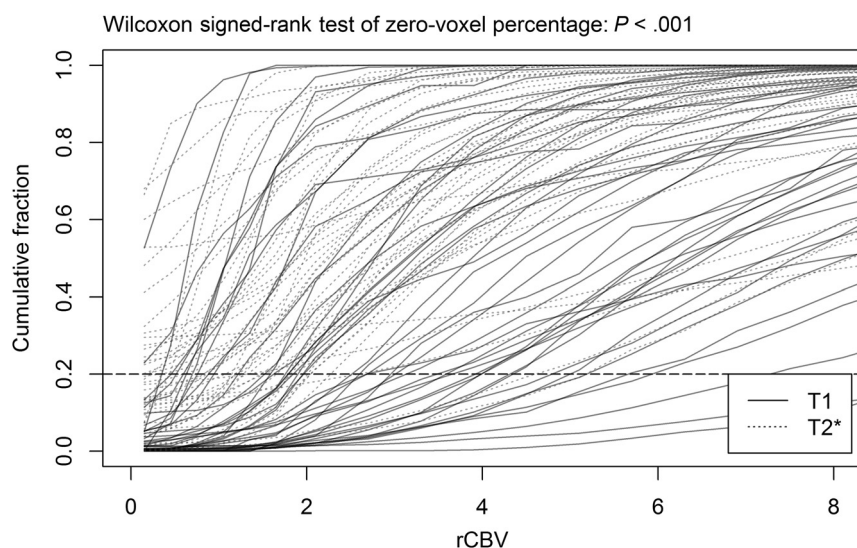


FIG 5. Cumulative histogram of T1- and T2*-rCBV values in all included examinations. With T2*-rCBV measurement, the leftmost beginning point of the cumulative fraction is >0.2 (horizontal dashed line) in 17 lesions (37.8%), implying that in each entire VOI of those lesions, more than one-fifth of the voxels contained rCBV values of <0.3 (the first bin of histogram). With T1-PWI-based rCBV measurements, in contrast, only 2 lesions (4.4%) show an initial cumulative fraction above 0.2.

DISCUSSION

In the current study, rCBV values were independently calculated using T1- and T2*-PWI in patients with postoperative high-grade gliomas, showing a positive correlation and fair consistency. The ICC was slightly lower than the previously reported values (0.56 versus 0.74).¹³ T1- and T2*-rCBV revealed a fine diagnostic performance in discriminating eventually progressed tumors from nonprogressive lesions (AUC = 0.811 and 0.793, respectively). The difference between AUCs was more pronounced in the subgroup with SSE (0.500 versus 0.750), though without statistical significance

($P = .117$). All results are covered by the range of previously reported AUC values (0.739–0.938) in the studies differentiating progression from pseudoprogression with the use of rCBV based on conventional T2*-PWI,^{5–7} except the T2*-rCBV results in examinations with SSE.

Most of the few previous studies involving T1-PWI validated its clinical significance based on glioma grading^{13,18–22} and reported calculated AUC values of 0.72–0.99.^{13,19,21} Only 1 study by Saini et al¹³ performed a statistical comparison of its diagnostic performance with T2*-rCBV in discriminating grade 3 and grade 4 gliomas, with no significant difference in AUC values (0.723 versus 0.767). In our results, T1- and T2*-rCBV similarly showed sufficient diagnostic performance in differentiating progressive from nonprogressive lesions. In another report by Larsen et al,¹⁷ evaluating the clinical usefulness of T1-PWI in discriminating tumor recurrence from radiation necrosis, rCBV was able to accurately detect all 3 regressing lesions of 14 classified lesions, strongly consistent with FDG-PET. Our T1-PWI also demonstrated 100% sensitivity in detecting recurrent lesions with acceptable specificity (57.1%). Additional Kaplan-Meier survival curves and genomic subclass analyses are provided in the Online Supplemental Data, also showing consistency with the well-known results of previous studies.^{9,27–29}

In the Bland-Altman plot comparing the 90th percentiles of the rCBV of both methods, 4 upper and 2 lower outliers were present, as previously suggested in Fig 4. VOIs of 2 upper and 2 lower outliers were located at the skull base and were disturbed by partial signal loss. One upper outlier with a pituitary stalk lesion (Online Supplemental Data) demonstrated a lower T2*-rCBV than the calculated cutoff value, being a false-negative case, while appropriately detected by T1-PWI. Another upper outlier was limited not only by its location but also due to considerable internal hemorrhage (Fig 2), with underestimation of T2*-rCBV due to a large area of signal loss. Marginal hemorrhage was also combined in the skull base lesions of the 2 lower outliers. Although rare, calcification was another source of T2*-PWI degradation, as shown in the Online Supplemental Data.

Several studies documented the rate of uninterpretable T2*-PWI owing to susceptibility-induced signal loss and geometric

Table 2: Summary of T1- and T2*-rCBV values distinguishing the progression group (n = 20) from the nonprogression group (n = 14)

Values	P Group (mean)	NP Group (mean)	P Value ^a	AUC	Cutoff ^b	Sensitivity	Specificity	P Value versus T1-rCBV ^c
T1-rCBV, 90th percentile	13.0 (SD, 6.9)	6.6 (SD, 6.1)	.008	0.811	4.930	100.0%	57.1%	
T2*-rCBV, 90th percentile	7.9 (SD, 4.0)	4.3 (SD, 3.1)	.009	0.793	4.453	90.0%	64.3%	.835

Note:—P Group indicates progression group; NP Group, nonprogression group.

^aIndependent t test.

^bYouden index.

^cDeLong test.

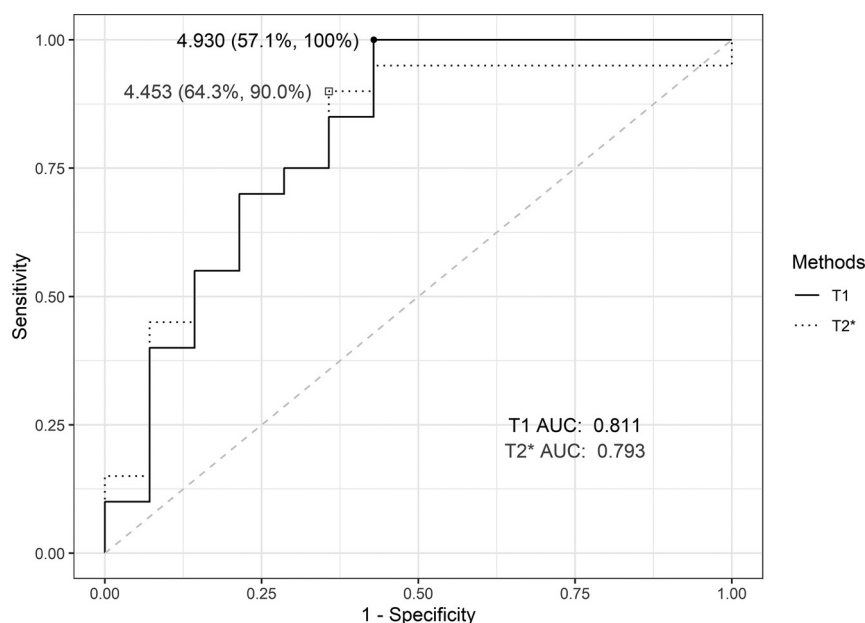


FIG 6. The ROC curves of T1- and T2*-rCBV using 90th percentile values. The AUC values of T1- and T2*-rCBV revealed no significant difference ($P = .835$).

distortion.^{11,12,30,31} A lower percentage of image degradation was seen in patients with preoperative gliomas (4.3%)³¹ than in postoperative populations (7.0%–10.9%).^{11,12,30} Compared with their results, our study demonstrated a slightly higher rate of SSE (20.0%, visualization grades 0–I on T2*-PWI). In the study by Saini et al¹³ involving a mixed population of preoperative and postoperative patients (43 and 6 patients, respectively), the rate of suboptimal T2*-PWI (visualization grades 0–II) was lower than in our patients (32.7% versus 71.1%). No previous studies were found, however, regarding the statistical comparison of signal loss between T1- and T2*-PWI. In our study, voxelwise analysis showed that postoperative T2*-PWI contained a significantly higher prevalence of signal loss than T1-PWI (17.7% versus 3.1%, respectively). In particular, T1-PWI showed a higher AUC value than T2*-PWI in the examinations with SSE (0.750 versus 0.500), though no significant difference was observed, possibly due to the small number of subgroups (3 examinations with progressed lesions, 4 examinations with nonprogressed lesions).

Only 2 previous studies directly compared the rCBV values obtained from T1- and T2*-based perfusion MR imaging in patients

with gliomas.^{13,19} In both studies, T1-rCBV values tended to be slightly lower than in conventional T2*-rCBV, contrary to our results. Saini et al¹³ also compared the consistency of T1- and T2*-rCBV measurements, reporting a higher ICC (0.74) between the 2 methods than in our result (0.56). Because both studies included more preoperative patients and used hotspot measurements of rCBV, avoiding areas with signal loss, histograms of T2*-rCBV values in our study might have been more affected by susceptibility effects, resulting in different T1- and T2*-rCBV relationships under postoperative circumstances than in those 2 previous reports. Although T2*-rCBV is a reasonable reference value obtained using the established method, because of its apparent partial inaccuracy due to susceptibility effects, other modalities may be considered the criterion standard for comparison. As previously mentioned, Larsen et al¹⁷

used FDG-PET to compare the clinical performance of T1-rCBV in surgically treated patients. Some recent articles compared amino acid PET with T2*-rCBV in posttreatment patients with gliomas to differentiate progression from treatment-related changes,^{32,33} and T1-rCBV may also be compared with amino acid PET in further studies. Likewise, arterial spin-labeling and amide proton transfer techniques are other candidates for clinical validation of T1-rCBV, in the same manner as in previous reports.^{34,35} Further investigations comparing T1-PWI with CT perfusion studies may yield data with higher reliability regarding its technical performance in postoperative cases.

The dynamic contrast-enhancement permeability analysis based on the extended Tofts model has also provided useful information in patients with gliomas. A meta-analysis by Liang et al³⁶ demonstrated that volume transfer constant (k^{trans}) and volume of extravascular extracellular space (V_e) were reliable parameters for glioma grading, while some studies also suggested the usefulness of k^{trans} and volume of blood plasma (V_p) in the differentiation of recurrence from treatment changes.^{6,37} With the high temporal resolution protocol suggested in our study, both traditional permeability

imaging and the T1-PWI-derived rCBV map can be acquired in a single scan, thereby allowing simultaneous analysis of permeability and hemodynamic properties of the tumor.

Our study has several limitations. This study was conducted retrospectively with a relatively small number of patients. The non-randomized patient assignment may have caused selection bias. Second, nordicICE enabled normalization of rCBV via automated WM segmentation without allowing manual selection of normal WM. Because the released perfusion analysis tool was optimized to T2*-weighted source images, WM masks produced by T1-PWI source images were suboptimal in some patients and carried a risk of error in the rCBV calculation. Additionally, Sahoo et al²¹ reported a slightly lower diagnostic accuracy of T1-rCBV calculated by the automated method compared with manual selection by the expert. Further software optimization is needed to provide appropriate CBV normalization.

Another technical limitation was the presence of aliasing artifacts with the use of parallel imaging in some source images of T1-PWI, caused by bright subcutaneous fat, which can be diminished by fat suppression or the low in-plane sensitivity encoding factor but requires a longer acquisition time. Parameter optimization regarding the trade-off of spatial and temporal resolution is important and may be further compensated for by using advanced artifact-free acceleration techniques in the future.

CONCLUSIONS

Relative CBV acquired from T1-based perfusion MR imaging with high temporal resolution showed a fine clinical performance in patients with postoperative high-grade gliomas, suggesting its potential role as a valid alternative to the traditional T2*-PWI. The relative clinical usefulness of T1-PWI compared with T2*-PWI might be more pronounced in examinations with SSE. Technically, T1- and T2*-PWI were fairly consistent in terms of calculated rCBV values. The prevalence of signal loss was significantly higher in T2*-PWI than in T1-PWI, which might have affected the consistency between the 2 methods. We suggest further validation of the T1-PWI in future studies for widespread application in susceptibility-prone situations.

Disclosure forms provided by the authors are available with the full text and PDF of this article at www.ajnr.org.

REFERENCES

1. Cha S, Johnson G, Wadghiri YZ, et al. **Dynamic, contrast-enhanced perfusion MRI in mouse gliomas: correlation with histopathology.** *Magn Reson Med* 2003;49:848–55 [CrossRef Medline](#)
2. Provenzale JM, Mukundan S, Barboriak DP. **Diffusion-weighted and perfusion MR imaging for brain tumor characterization and assessment of treatment response.** *Radiology* 2006;239:632–49 [CrossRef Medline](#)
3. Aronen HJ, Gazit IE, Louis DN, et al. **Cerebral blood volume maps of gliomas: comparison with tumor grade and histologic findings.** *Radiology* 1994;191:41–51 [CrossRef Medline](#)
4. Law M, Yang S, Babb JS, et al. **Comparison of cerebral blood volume and vascular permeability from dynamic susceptibility contrast-enhanced perfusion MR imaging with glioma grade.** *AJNR Am J Neuroradiol* 2004;25:746–55 [Medline](#)
5. Young RJ, Gupta A, Shah AD, et al. **MRI perfusion in determining pseudoprogression in patients with glioblastoma.** *Clin Imaging* 2013;37:41–49 [CrossRef Medline](#)
6. Shin KE, Ahn KJ, Choi HS, et al. **DCE and DSC MR perfusion imaging in the differentiation of recurrent tumour from treatment-related changes in patients with glioma.** *Clin Radiol* 2014;69:e264–72 [CrossRef Medline](#)
7. Prager AJ, Martinez N, Beal K, et al. **Diffusion and perfusion MRI to differentiate treatment-related changes including pseudoprogression from recurrent tumors in high-grade gliomas with histopathologic evidence.** *AJNR Am J Neuroradiol* 2015;36:877–85 [CrossRef Medline](#)
8. Wan B, Wang S, Tu M, et al. **The diagnostic performance of perfusion MRI for differentiating glioma recurrence from pseudoprogression: a meta-analysis.** *Medicine (Baltimore)*. 2017;96:e6333 [CrossRef Medline](#)
9. Law M, Young RJ, Babb JS, et al. **Gliomas: Predicting time to progression or survival with cerebral blood volume measurements at dynamic susceptibility-weighted contrast-enhanced perfusion MR imaging.** *Radiology* 2008;247:490–98 [CrossRef Medline](#)
10. Jahng GH, Li KL, Ostergaard L, et al. **Perfusion magnetic resonance imaging: a comprehensive update on principles and techniques.** *Korean J Radiol* 2014;15:554–77 [CrossRef Medline](#)
11. Heo YJ, Kim HS, Park JE, et al. **Uninterpretable dynamic susceptibility contrast-enhanced perfusion MR images in patients with post-treatment glioblastomas: cross-validation of alternative imaging options.** *PLoS One* 2015;10:e0136380 [CrossRef Medline](#)
12. Hu LS, Baxter LC, Smith KA, et al. **Relative cerebral blood volume values to differentiate high-grade glioma recurrence from post-treatment radiation effect: direct correlation between image-guided tissue histopathology and localized dynamic susceptibility-weighted contrast-enhanced perfusion.** *AJNR Am J Neuroradiol* 2009;30:552–58 [CrossRef Medline](#)
13. Saini J, Gupta RK, Kumar M, et al. **Comparative evaluation of cerebral gliomas using rCBV measurements during sequential acquisition of T1-perfusion and T2-perfusion MRI.** *PLoS One* 2019;14:e0215400 [CrossRef Medline](#)
14. Dean BL, Lee C, Kirsch JE, et al. **Cerebral hemodynamics and cerebral blood volume: MR assessment using gadolinium contrast agents and T1-weighted turbo-FLASH imaging.** *AJNR Am J Neuroradiol* 1992;13:39–48 [Medline](#)
15. Hackländer T, Reichenbach JR, Hofer M, et al. **Measurement of cerebral blood volume via the relaxing effect of low-dose gadopentetate dimeglumine during bolus transit.** *AJNR Am J Neuroradiol* 1996;17:821–30 [Medline](#)
16. Sourbron S, Ingrisch M, Siefert A, et al. **Quantification of cerebral blood flow, cerebral blood volume, and blood-brain-barrier leakage with DCE-MRI.** *Magn Reson Med* 2009;62:205–17 [CrossRef Medline](#)
17. Larsen VA, Simonsen HJ, Law I, et al. **Evaluation of dynamic contrast-enhanced T1-weighted perfusion MRI in the differentiation of tumor recurrence from radiation necrosis.** *Neuroradiology* 2013;55:361–69 [CrossRef Medline](#)
18. Roy B, Gupta RK, Maudsley AA, et al. **Utility of multiparametric 3-T MRI for glioma characterization.** *Neuroradiology* 2013;55:603–13 [CrossRef Medline](#)
19. Falk A, Fahlström M, Rostrup E, et al. **Discrimination between glioma grades II and III in suspected low-grade gliomas using dynamic contrast-enhanced and dynamic susceptibility contrast perfusion MR imaging: a histogram analysis approach.** *Neuroradiology* 2014;56:1031–38 [CrossRef Medline](#)
20. Gupta PK, Saini J, Sahoo P, et al. **Role of dynamic contrast-enhanced perfusion magnetic resonance imaging in grading of pediatric brain tumors on 3T.** *Pediatr Neurosurg* 2017;52:298–305 [CrossRef Medline](#)
21. Sahoo P, Gupta RK, Gupta PK, et al. **Diagnostic accuracy of automatic normalization of CBV in glioma grading using T1-weighted DCE-MRI.** *Magn Reson Imaging* 2017;44:32–37 [CrossRef Medline](#)
22. Sengupta A, Ramaniharan AK, Gupta RK, et al. **Glioma grading using a machine-learning framework based on optimized features obtained from T1 perfusion MRI and volumes of tumor components.** *J Magn Reson Imaging* 2019;50:1295–306 [CrossRef Medline](#)

23. Conte GM, Castellano A, Altabella L, et al. Reproducibility of dynamic contrast-enhanced MRI and dynamic susceptibility contrast MRI in the study of brain gliomas: a comparison of data obtained using different commercial software. *Radiol Med* 2017;122:294–302 [CrossRef Medline](#)
24. Conte GM, Altabella L, Castellano A, et al. Comparison of T1 mapping and fixed T1 method for dynamic contrast-enhanced MRI perfusion in brain gliomas. *Eur Radiol* 2019;29:3467–79 [CrossRef Medline](#)
25. Tietze A, Mouridsen K, Mikkelsen IK. The impact of reliable prebolus T1 measurements or a fixed T1 value in the assessment of glioma patients with dynamic contrast enhancing MRI. *Neuroradiology* 2015;57:561–72 [CrossRef Medline](#)
26. Koo TK, Li MY. A guideline of selecting and reporting intraclass correlation coefficients for reliability research. *J Chiropr Med* 2016;15:155–63 [CrossRef Medline](#)
27. Gahramanov S, Muldoon LL, Varallyay CG, et al. Pseudoprogression of glioblastoma after chemo- and radiation therapy: diagnosis by using dynamic susceptibility-weighted contrast-enhanced perfusion MR imaging with ferumoxytol versus gadoteridol and correlation with survival. *Radiology* 2013;266:842–52 [CrossRef Medline](#)
28. Álvarez-Torres M del M, Fuster-García E, Juan-Albarracín J, et al. Local detection of microvessels in IDH-wildtype glioblastoma using relative cerebral blood volume: an imaging marker useful for astrocytoma grade 4 classification. *BMC Cancer* 2022;22:40 [CrossRef Medline](#)
29. Wang K, Li Y, Cheng H, et al. Perfusion CT detects alterations in local cerebral flow of glioma related to IDH, MGMT and TERT status. *BMC Neurol* 2021;21:460 [CrossRef Medline](#)
30. Mangla R, Singh G, Ziegelitz D, et al. Changes in relative cerebral blood volume 1 month after radiation-temozolomide therapy can help predict overall survival in patients with glioblastoma. *Radiology* 2010;256:575–84 [CrossRef Medline](#)
31. Nguyen TB, Cron GO, Perdrizet K, et al. Comparison of the diagnostic accuracy of DSC- and dynamic contrast-enhanced MRI in the preoperative grading of astrocytomas. *AJNR Am J Neuroradiol* 2015;36:2017–22 [CrossRef Medline](#)
32. Paprottka KJ, Kleiner S, Preibisch C, et al. Fully automated analysis combining [18F]-FET-PET and multiparametric MRI including DSC perfusion and APTw imaging: a promising tool for objective evaluation of glioma progression. *Eur J Nucl Med Mol Imaging* 2021;48:4445–55 [CrossRef Medline](#)
33. Steidl E, Langen KJ, Hmeidan SA, et al. Sequential implementation of DSC-MR perfusion and dynamic [18F]FET PET allows efficient differentiation of glioma progression from treatment-related changes. *Eur J Nucl Med Mol Imaging* 2021;48:1956–65 [CrossRef Medline](#)
34. Choi YJ, Kim HS, Jahng GH, et al. Pseudoprogression in patients with glioblastoma: Added value of arterial spin labeling to dynamic susceptibility contrast perfusion MR imaging. *Acta Radiol* 2013;54:448–54 [CrossRef Medline](#)
35. Park YW, Ahn SS, Kim EH, et al. Differentiation of recurrent diffuse glioma from treatment-induced change using amide proton transfer imaging: incremental value to diffusion and perfusion parameters. *Neuroradiology* 2021;63:363–72 [CrossRef Medline](#)
36. Liang J, Liu D, Gao P, et al. Diagnostic values of DCE-MRI and DSC-MRI for differentiation between high-grade and low-grade gliomas: a comprehensive meta-analysis. *Acad Radiol* 2018;25:338–48 [CrossRef Medline](#)
37. Thomas AA, Arevalo-Perez J, Kaley T, et al. Dynamic contrast enhanced T1 MRI perfusion differentiates pseudoprogression from recurrent glioblastoma. *J Neurooncol* 2015;125:183–90 [CrossRef Medline](#)